Production cross sections of samarium-153 and -145 via alpha-particle-induced reactions on natural neodymium

Masayuki Aikawa[1,2,3,*], Michiya Sakaguchi[2], Naoyuki Ukon[4], Yukiko Komori[5], Hiromitsu Haba[5], Naohiko Otuka[6] and Sándor Takács[7]

[1] *Faculty of Science, Hokkaido University, Sapporo 060-0810, Japan*

[2] *Graduate School of Biomedical Science and Engineering, Hokkaido University, Sapporo 060-8638, Japan*

[3] *Global Center for Biomedical Science and Engineering, Faculty of Medicine, Hokkaido University, Sapporo 060-8648, Japan*

[4] *Advanced Clinical Research Center, Fukushima Medical University, Fukushima 960-1295, Japan*

[5] *Nishina Center for Accelerator-Based Science, RIKEN, Wako 351-0198, Japan*

[6] *Nuclear Data Section, Division of Physical and Chemical Sciences, Department of Nuclear Sciences and Applications, International Atomic Energy Agency, A-1400 Wien, Austria*

[7] *Institute for Nuclear Research, ATOMKI, 4026 Debrecen, Hungary*

Abstract

Production cross sections of ^{153,145}Sm via alpha-particle-induced reactions on ^{nat}Nd were measured up to 23 MeV. The stacked-foil activation technique and high-resolution gamma-ray spectrometry were adopted for the measurement. The obtained cross sections were compared with the literature data and the TENDL-2019 and TENDL-2021 values. Physical thick target yields of the two radionuclides were derived from the measured cross sections.

Keyword

Samarium-153, Samarium-145, Alpha irradiation, Neodymium target, Cross section

1. Introduction

Samarium radionuclides ^{153}Sm ($T_{1/2}$ = 46.3 h) and ^{145}Sm ($T_{1/2}$ = 340 d) can be used for treatment of bone metastases (Finlay et al., 2005) and for brachytherapy (Fairchild et al., 1987; Meigooni and Nath, 1992), respectively. Among possible production reactions of the two medical radionuclides, we have recently investigated alpha-particle-induced reactions on natural neodymium up to 50 MeV (Sakaguchi et al., 2021). The isotopic composition of natural neodymium is ^{142}Nd: 27.153%, ^{143}Nd: 12.173%, ^{144}Nd: 23.798%, ^{145}Nd: 8.293%, ^{146}Nd: 17.189%, ^{148}Nd: 5.756%, and ^{150}Nd: 5.638%,

[*] Corresponding author: Masayuki AIKAWA (aikawa@sci.hokudai.ac.jp), Faculty of Science, Hokkaido University, Sapporo 060-0810, Japan

respectively (Meija et al., 2016). It was found that our measured cross sections of the ^{nat}Nd(α,x)^{153}Sm reaction were, however, largely deviated from the experimental data published earlier (Qaim et al., 2007). The peak amplitudes of the cross sections differ from each other by a factor of more than two. In addition, for the ^{nat}Nd(α,x)^{145}Sm reaction no experimental study other than our previous one was found in the literature survey. Therefore, we decided to conduct additional independent experiments up to 23 MeV to increase reliability of the production cross sections of ^{153,145}Sm. The alpha-particle energy of 23 MeV was selected to focus on the peak region of the excitation function of the ^{nat}Nd(α,x)^{153}Sm reaction at around 18 MeV and the ^{nat}Nd(α,x)^{145}Sm reaction at around 20 MeV. The incident beam energy of 29 MeV was reduced to 23 MeV through several Ti foils. The newly measured cross sections were compared with the previous studies and the values in the TENDL-2019 and new TENDL-2021 libraries (Koning et al., 2019). The physical thick target yields for production of ^{153,145}Sm were derived using the fitted curve over the experimental cross sections.

2. Experimental

Two experiments (#1 and #2) were performed using 29-MeV alpha-particle beams at the RIKEN AVF cyclotron. The stacked-foil activation technique and high-resolution gamma-ray spectrometry were adopted for the experiments. Two targets for the experiments were composed of pure metallic foils of ^{nat}Nd (99.0% purity, nominal 25-μm thick, Goodfellow Co., Ltd., UK) and ^{nat}Ti (99.6% purity, nominal 5-μm thick, Nilaco Corp., Japan). The ^{nat}Ti foils were placed in the stacks to assess beam parameters and energy degradation in the targets using the ^{nat}Ti(α,x)^{51}Cr monitor reaction. The lateral size and weight of the original foils were measured, and average thicknesses were derived for both foils. To suppress the oxidation effect of the Nd foil, the weight of the foil was measured soon after unsealing. The derived average thicknesses of the ^{nat}Nd and ^{nat}Ti foils were 16.7 and 2.25 mg/cm^2, respectively. The original foils were then cut into a size of 10×10 mm to compose the stacked targets that fit into Faraday-cup like target holders. Six ^{nat}Nd and fourteen ^{nat}Ti foils were stacked in both targets in different orders. The configuration of the two stacked targets is listed in Table. 1. Both targets were arranged in three groups of Ti, Nd and Ti foils. The aim of this arrangement was to be able to check the beam intensity with the Ti group at the high energy, to check the energy loss calculations of the alpha-particles in the stacks using the Ti group at the low energy and to have the cross section data points for the selected reactions on Nd around the maximum of the excitation function.

Each target was irradiated for 33 min with an alpha-particle beam. The incident beam energy was 28.9±0.2 MeV identically in both irradiations. The beam energy was measured by the time-of-flight method (Watanabe et al., 2014). The energy degradation of the beam in the stacked targets was calculated using stopping powers obtained from the SRIM code (Ziegler et al., 2008). The average beam intensities measured by the Faraday cups were 205 nA (#1) and 209 nA (#2), respectively. The experimental parameters for easy comparison are summarized in Table 2.

Gamma rays emitted from the activated foils were measured without chemical separation using high-purity germanium detectors (ORTEC GMX30P4-70). The efficiency of the detector was obtained using a multiple gamma-ray point source with ^{57,60}Co, ^{85}Sr, ^{88}Y, ^{109}Cd, ^{113}Sn, ^{137}Cs, ^{139}Ce, ^{203}Hg, and ^{241}Am (Eckert & Ziegler Isotope Products). The measurement of the gamma rays was performed three times for every foil as listed in Table 2. The last series of the measurement (Ser. 3) was adopted for deduction of the cross sections. The other series (Ser. 1 and 2) were used to cross-check the cross sections. Both targets consisted of two groups of Ti foils and one group of Nd foils. The spectra measured for the first foil of each group were not used in data evaluation because of the recoil effect. Spectra measured for the rest of the foils are considered to be recoil-compensated, as the recoil effect has no strong energy dependence on adjacent foils in the same group. The nuclear reaction and decay data used to deduce activation cross sections are listed in Table 3, retrieved from the online databases, NuDat 3.0 (National Nuclear Data Center, 2021) and QCalc (Pritychenko and Sonzogni, 2003).

To derive the cross section σ (cm^2), the following equation was used,

$$\sigma = \frac{\lambda}{n_t I_\alpha} \frac{N_\gamma}{\varepsilon_d \varepsilon_\gamma \varepsilon_t (1 - e^{-\lambda T_b}) e^{-\lambda T_c} (1 - e^{-\lambda T_m})}$$

where λ is the decay constant of each radionuclide (s^{-1}), n_t is the surface density of target atoms (cm^{-2}), I_α is the alpha-particle-beam intensity (s^{-1}), N_γ is the net count of the gamma-ray peak, ε_d is the detector efficiency, ε_γ is the gamma-ray intensity, ε_t is the dead time correction, T_b, T_c and T_m are the irradiation, cooling and acquisition times (s), respectively.

Cross sections of the ^{nat}Ti(α,x)^{51}Cr monitor reaction were derived for assessment of the beam parameters and the target thicknesses. The measurement of gamma rays at 320.08 keV (I_γ = 9.91%) was used to derive the cross sections. The obtained cross sections were compared with the IAEA recommended values (Hermanne et al., 2018; Tárkányi et al., 2007). The deduced cross sections of the Ti foils in the high energy group were used to check the beam intensities. For good agreement with the recommended values the initial beam intensity of the second experiment (#2) measured by the Faraday cup was corrected by +2%. Using the Ti foils in the low energy group the energy loss of the beam was checked and for the good agreement with the recommended values the thickness of the ^{nat}Nd foil was decreased by 2% and the initial bombarding energy measured by the time-of-flight method was increased by 0.2 MeV. The beam intensity of the first experiment (#1) and the measured thickness of the ^{nat}Ti foil were adopted without any correction. The deduced cross sections for the ^{nat}Ti(α,x)^{51}Cr reaction using the corrected experimental parameters are compared with the IAEA recommended values in Fig. 1 and found in good agreement with the values in 2007 (Tárkányi et al., 2007) at the high energy region. The corrected parameters listed in Table 2 were used in data evaluation.

3. Results and discussion

Activation cross sections of the $^{nat}Nd(\alpha,x)^{153,145}Sm$ reactions were determined. The derived cross sections are summarized in Tables 4 and 5 and graphically shown in Figs. 2 and 3 with the literature data and the theoretical prediction of the TENDL-2019 and TENDL-2021 libraries (Koning et al., 2019). Physical thick target yields were deduced using the fit over the measured cross sections.

The median projectile energy and its uncertainty with the total energy loss in parentheses in each foil are listed in Tables 4 and 5. The calculated energy loss in the Nd foils increases from 2.1 to 3.0 MeV. The total uncertainty of the energy increases from 0.3 MeV to 0.5 MeV in both cases (#1 and #2). The total uncertainty of the cross sections (7.5-8.9%) were derived from the square root of the quadratic sum of the partial uncertainties: beam intensity (5%), gamma-ray intensity (0.8%), detector efficiency (5%), target thickness (2%), target purity (1%) and counting statistics (0.4-5.5%).

3.1 The $^{nat}Nd(\alpha,x)^{153}Sm$ reaction

Production cross sections of ^{153}Sm ($T_{1/2}$ = 46.3 h) via alpha-particle-induced reactions on natural neodymium were determined. In a natural neodymium target only the (α,p) reaction on ^{150}Nd (E_{th} = 6.9 MeV) can contribute to direct formation of ^{153}Sm. In the measurement also the indirect formation via decay of ^{153}Pm ($T_{1/2}$ = 5.25 min), produced in the $^{150}Nd(\alpha,p)^{153}Pm$ reaction (E_{th} = 8.1 MeV), is included. Accordingly the derived cross sections are cumulative cross sections. The cross sections measured on natural neodymium can be normalized by the abundance to those on ^{150}Nd and vice versa. The net counts of the gamma line at 103.18 keV (I_γ = 29.25%) emitted with the decay of ^{153}Sm were measured after cooling times of 6.0-19.5 h (#1) and 10.9-24.9 h (#2) when the precursor ^{153}Pm had completely decayed to ^{153}Sm. The attenuation of the 103.18-keV low-energy gamma line was calculated using the X-ray mass attenuation coefficients (Hubbel and Seltzer, 2004). The attenuation of the 103.18-keV gamma line in the Nd foil was estimated to be 2.1%. The cumulative cross sections were determined using the net counts corrected for attenuation.

The deduced cross sections are shown in Fig. 2 in comparison with the literature data (Qaim et al., 2007; Sakaguchi et al., 2021) and the TENDL-2019 and TENDL-2021 values (Koning et al., 2019). The present results agree with each other (#1 and #2) and also with our previous study (Sakaguchi et al., 2021). However, the only other available literature data (Qaim et al., 2007) are too high. Based on the newly obtained results, the smaller cross sections seem to be more reliable. The TENDL-2019 values are too low when comparing to our experimental data, however, data taken from the updated TENDL-2021 library are higher and more consistent with our results.

3.2 The $^{nat}Nd(\alpha,x)^{145}Sm$ reaction

The longer-lived ^{145}Sm ($T_{1/2}$ = 340 d) can be produced below 23 MeV on two stable isotopes of natural neodymium (^{142}Nd: 27.153% and ^{143}Nd: 12.173%) in the $^{142}Nd(\alpha,n)^{145}Sm$ and

$^{143}Nd(\alpha,2n)^{145}Sm$ reactions. No contribution of the $^{144}Nd(\alpha,3n)^{145}Sm$ reaction is expected, since its threshold energy is 25.6 MeV. For data analysis the only intense gamma line at 61.23 keV (I_γ = 12.15%) was used. The measured net counts were corrected by +8.4% taking into account the attenuation of this low-energy gamma line in the Nd foil. The cross sections derived using the corrected counts are listed in Tables 4 and 5 and graphically presented in Fig 3.

The newly determined cross sections are consistent with the experimental data published earlier (Sakaguchi et al., 2021) and the TENDL-2019 and TENDL-2021 values (Koning et al., 2019). The updated TENDL-2021 library provides the same predicted curve up to 30 MeV as the earlier one, though at higher energies a slight difference is seen between the TENDL-2019 and TENDL-2021 values.

3.3 Physical thick target yields

Physical thick target yields (Otuka and Takács, 2015) of $^{153,145}Sm$ via alpha-particle-induced reactions on natural neodymium were deduced using fitted curves of the excitation functions measured in the present study and in our previous work (Sakaguchi et al., 2021) and stopping powers calculated using the SRIM code (Ziegler et al., 2008). The yield of ^{153}Sm via the reaction on ^{150}Nd was also deduced from those on ^{nat}Nd. The three deduced yields are shown in Fig. 4. The yields of $^{153,145}Sm$ on ^{nat}Nd and that of ^{153}Sm on ^{150}Nd can reach 6.39, 5.44 and 113 MBq/C (19.6, 2.30, and 408 kBq/μAh) at 30 MeV, respectively.

4. Summary

We determined the excitation functions of alpha-particle-induced reactions on ^{nat}Nd for the formation of $^{145,153}Sm$ radionuclides. The experiments were performed at the RIKEN AVF cyclotron using the stacked-foil activation technique and high-resolution gamma-ray spectrometry. The activation cross sections of $^{145,153}Sm$ were determined and compared with the literature data and theoretical prediction in the TENDL-2019 and TENDL-2021 libraries. The newly obtained results in this work are consistent with our previous study. The yields of $^{145,153}Sm$ on ^{nat}Nd are 6.39 and 5.44 MBq/C (19.6 and 2.30 kBq/μAh) at 30 MeV, respectively. The yield of ^{153}Sm using enriched ^{150}Nd targets can reach 113 MBq/C (408 kBq/μAh) at 30 MeV. The deduced yield of ^{153}Sm indicates that irradiation with a high intensity for a long period is required to obtain the commonly used dose (37 MBq/kg) of ^{153}Sm-EDTMP (Finlay et al., 2005).

Declaration of Competing Interest

The authors have no conflicts of interest in this paper.

Acknowledgments

This work was performed at the RI Beam Factory operated by RIKEN Nishina Center and CNS, University of Tokyo.

References

Fairchild, R.G., Kalef-Ezra, J., Packer, S., Wielopolski, L., Laster, B.H., Robertson, J.S., Mausner, L., Kanellitsas, C., 1987. Samarium-145: A new brachytherapy source. Phys. Med. Biol. 32, 847–858. https://doi.org/10.1088/0031-9155/32/7/005

Finlay, I.G., Mason, M.D., Shelley, M., 2005. Radioisotopes for the palliation of metastatic bone cancer: a systematic review. Lancet Oncol. 6, 392–400. https://doi.org/10.1016/S1470-2045(05)70206-0

Hermanne, A., Ignatyuk, A. V., Capote, R., Carlson, B. V., Engle, J.W., Kellett, M.A., Kibédi, T., Kim, G., Kondev, F.G., Hussain, M., Lebeda, O., Luca, A., Nagai, Y., Naik, H., Nichols, A.L., Nortier, F.M., Suryanarayana, S. V., Takács, S., Tárkányi, F.T., Verpelli, M., 2018. Reference Cross Sections for Charged-particle Monitor Reactions. Nucl. Data Sheets 148, 338–382. https://doi.org/10.1016/j.nds.2018.02.009. Data available at https://www-nds.iaea.org/medical/monitor_reactions.html

Hubbel, J.H., Seltzer, S.M., 2004. X-Ray Mass Extinction Coefficients [WWW Document]. NIST Stand. Ref. Database 126. https://doi.org/https://doi.org/10.18434/T4D01F

Koning, A.J., Rochman, D., Sublet, J., Dzysiuk, N., Fleming, M., Marck, S. van der, 2019. TENDL: Complete Nuclear Data Library for Innovative Nuclear Science and Technology. Nucl. Data Sheets 155, 1–55. https://doi.org/10.1016/j.nds.2019.01.002

Meigooni, A.S., Nath, R., 1992. A comparison of radial dose functions for ^{103}Pd, ^{125}I, ^{145}Sm, ^{241}Am, ^{169}Yb, ^{192}Ir, and ^{137}Cs brachytherapy sources. Int. J. Radiat. Oncol. Biol. Phys. 22, 1125–1130. https://doi.org/10.1016/0360-3016(92)90819-4

Meija, J., Coplen, T.B., Berglund, M., Brand, W.A., De Bièvre, P., Gröning, M., Holden, N.E., Irrgeher, J., Loss, R.D., Walczyk, T., Prohaska, T., 2016. Isotopic compositions of the elements 2013 (IUPAC Technical Report). Pure Appl. Chem. 88, 293–306. https://doi.org/10.1515/pac-2015-0503

National Nuclear Data Center, 2021. Nuclear structure and decay data on-line library, Nudat 3.0 [WWW Document]. URL http://www.nndc.bnl.gov/nudat3/

Otuka, N., Takács, S., 2015. Definitions of radioisotope thick target yields. Radiochim. Acta 103, 1–6. https://doi.org/10.1515/ract-2013-2234

Pritychenko, B., Sonzogni, A., 2003. Q-value Calculator (QCalc) [WWW Document]. URL http://www.nndc.bnl.gov/qcalc/

Qaim, S.M., Spahn, I., Kandil, S.A., Coenen, H.H., 2007. Nuclear data for production of ^{88}Y, ^{140}Nd, ^{153}Sm and ^{169}Yb via novel routes. Radiochim. Acta 95, 313–317. https://doi.org/10.1524/ract.2007.95.6.313

Sakaguchi, M., Aikawa, M., Ukon, N., Komori, Y., Haba, H., Otuka, N., Takács, S., 2021. Activation cross section measurement of alpha-particle induced reactions on natural neodymium. Appl. Radiat. Isot. 176, 109826. https://doi.org/10.1016/j.apradiso.2021.109826

Tárkányi, F., Takács, S., Gul, K., Hermanne, A., Mustafa, M.G., Nortier, M., Obložinský, P., Qaim, S.M., Scholten, B., Shubin, Y.N., Zhuang, Y., 2007. Monitor Reactions 2007, updated version of charged particle cross-section database for medical radioisotope production, IAEA-TECDOC-1211 [WWW Document]. URL https://www-nds.iaea.org/medical/medical-old/monitor_reactions.html

Watanabe, T., Fujimaki, M., Fukunishi, N., Imao, H., Kamigaito, O., Kase, M., Komiyama, M., Sakamoto, N., Suda, K., Wakasugi, M., Yamada, K., 2014. Beam energy and longitudinal beam profile measurement system at the RIBF, in: Proceedings of the 5th International Particle Accelerator Conference (IPAC 2014). pp. 3566–3568.

Ziegler, J.F., Biersack, J.P., Ziegler, M.D., 2008. SRIM: the Stopping and Range of Ions in Matter [WWW Document]. URL http://www.srim.org

Tables

Table 1. Foil configuration of each stacked target.

No.	Stack (#1)	Stack (#2)	No.	Stack (#1)	Stack (#2)
1	Ti	Ti	11	Nd	Nd
2	Ti	Ti	12	Nd	Nd
3	Ti	Ti	13	Nd	Nd
4	Ti	Ti	14	Nd	Nd
5	Ti	Ti	15	Nd	Nd
6	Ti	Ti	16	Nd	Ti
7	Ti	Ti	17	Ti	Ti
8	Ti	Ti	18	Ti	Ti
9	Ti	Ti	19	Ti	Ti
10	Ti	Nd	20	Ti	Ti

Table 2. Experimental parameters.

	#1	**#2**
Target		
Measured (corrected) thickness (mg/cm^2)	^{nat}Nd: 16.7 (16.3)	^{nat}Nd: 16.7 (16.3)
	^{nat}Ti: 2.25	^{nat}Ti: 2.25
Stack composition	10 Ti foils, 6 Nd foils and 4 Ti foils	9 Ti foils, 6 Nd foils and 5 Ti foils
Beam		
Measured (corrected) beam current (nA)	205±10	209 (213±10)
Primary energy (MeV)	28.9 (29.1±0.2)	28.9 (29.1±0.2)
Irradiation period (min)	33.0	33.0
Measurements		
Series: Cooling time (distance, dead time)	Ser. 1: 2.9-3.6 h (5 cm, <0.3%)	Ser. 1: 1.5-2.2 h (5 cm, 0.1-0.7%)
	Ser. 2: 3.8-5.0 h (3 cm, <0.3%)	Ser. 2: 2.4-3.6 h (3 cm, 0.1-0.6%)
	Ser. 3: 6.0-19.5 h (3 cm, <0.1%)	Ser. 3: 10.9-24.9 h (3 cm, <0.2%)

Table 3. Nuclear reaction and decay data of reaction products in this experiment retrieved from the online databases, NuDat 3.0 (National Nuclear Data Center, 2021) and QCalc (Pritychenko and Sonzogni, 2003).

Radionuclide	Decay mode	Half-life	Eγ (keV)	Iγ (%)	Contributing reactions	Q-value (MeV)	Threshold energy (MeV)
^{153}Sm	β^-: 100%	46.284(4) h	103.18012(17)	29.25(22)	^{150}Nd(α,n)	-6.8	6.9
					^{153}Pm decay	-7.9	8.1
^{145}Sm	ε: 100%	340(3) d	61.2265(17)	12.15(10)	^{144}Nd(α,3n)	-24.9	25.6
					^{143}Nd(α,2n)	-17.1	17.5
					^{142}Nd(α,n)	-10.9	11.3
^{51}Cr	ε: 100%	27.704(3) d	320.0824(4)	9.910(10)	^{47}Ti(α,γ)	8.9	0.0
					^{48}Ti(α,n)	-2.7	2.9
					^{49}Ti(α,2n)	-10.8	11.7
					^{50}Ti(α,3n)	-21.8	23.5

Table 4. Production cross sections derived in the first experiment (#1) in terms of the median projectile energy with total uncertainty and energy loss in parentheses in the unit of MeV.

	Cross section (mb)	
E (MeV)	^{153}Sm	^{145}Sm
22.6 ±0.3 (2.1)	0.92 ±0.07	169 ±13
20.6 ±0.3 (2.2)	0.96 ±0.07	168 ±13
18.3 ±0.3 (2.4)	1.21 ±0.09	94 ±7
15.9 ±0.4 (2.6)	1.02 ±0.08	19 ±2
13.3 ±0.5 (3.0)	0.17 ±0.01	

Table 5. Production cross sections derived in the second experiment (#2) in terms of the median projectile energy with total uncertainty and energy loss in parentheses in the unit of MeV.

	Cross section (mb)	
E (MeV)	^{153}Sm	^{145}Sm
23.0 ±0.3 (2.1)	0.93 ±0.07	168 ±13
21.0 ±0.3 (2.2)	0.99 ±0.07	171 ±13
18.8 ±0.3 (2.4)	1.21 ±0.09	102 ±8
16.4 ±0.4 (2.6)	1.12 ±0.08	22 ±2
13.8 ±0.5 (3.0)	0.27 ±0.02	

Figure captions

Fig. 1. Excitation function of the $^{nat}Ti(\alpha,x)^{51}Cr$ monitor reaction in comparison with the IAEA recommended values (Hermanne et al., 2018; Tárkányi et al., 2007).

Fig. 2. Excitation function of the $^{nat}Nd(\alpha,x)^{153}Sm$ reaction with the literature data (Qaim et al., 2007; Sakaguchi et al., 2021) and the TENDL-2019 and TENDL-2021 values (Koning et al., 2019).

Fig. 3. Excitation function of the $^{nat}Nd(\alpha,x)^{145}Sm$ reaction with the literature data (Sakaguchi et al., 2021) and the TENDL-2019 and TENDL-2021 values (Koning et al., 2019).

Fig. 4. Physical thick target yields of $^{153,145}Sm$ via alpha-particle-induced reactions on ^{nat}Nd and ^{150}Nd.

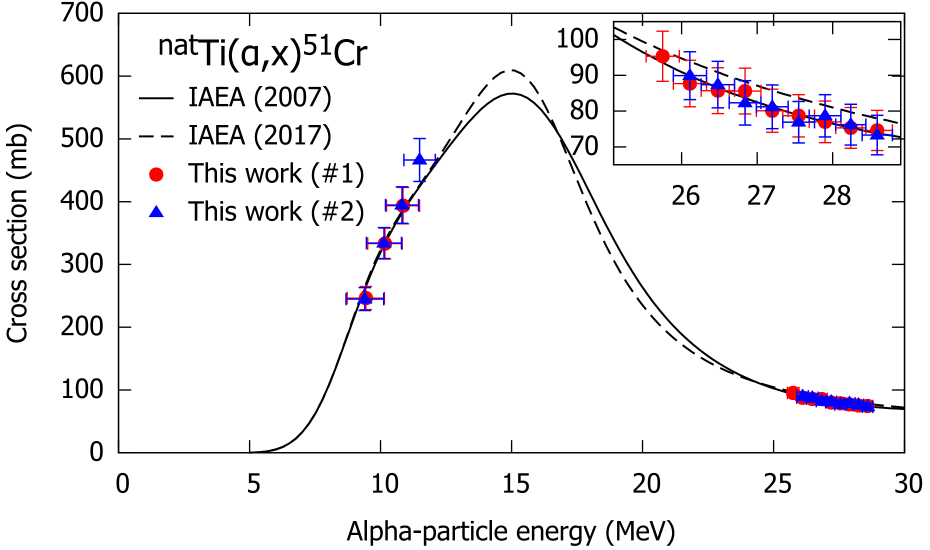

natTi(α,x)51Cr
IAEA (2007)
IAEA (2017)
This work (#1)
This work (#2)
Cross section (mb)
Alpha-particle energy (MeV)
0
100
200
300
400
500
600
700
0
5
10
15
20
25
30
100
90
80
70
26
27
28

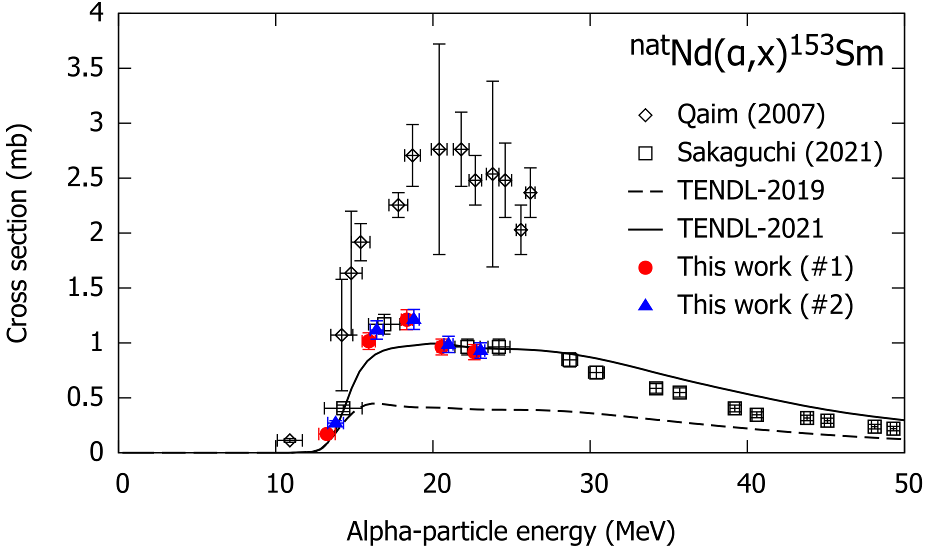

$^{nat}Nd(\alpha,x)^{153}Sm$
Qaim (2007)
Sakaguchi (2021)
TENDL-2019
TENDL-2021
This work (#1)
This work (#2)
Cross section (mb)
Alpha-particle energy (MeV)
0
0.5
1
1.5
2
2.5
3
3.5
4
0
10
20
30
40
50

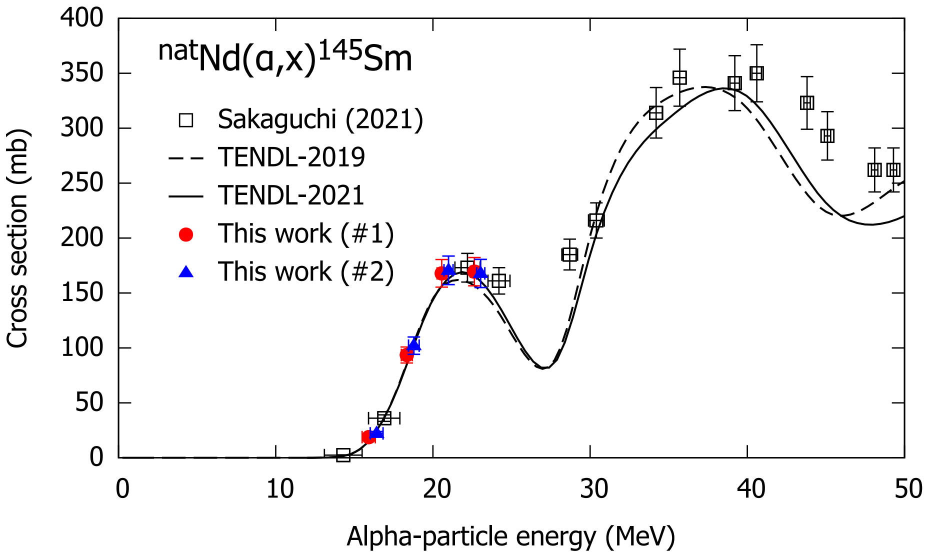

natNd(α,x)145Sm
Sakaguchi (2021)
TENDL-2019
TENDL-2021
This work (#1)
This work (#2)
Cross section (mb)
Alpha-particle energy (MeV)
0
50
100
150
200
250
300
350
400
0
10
20
30
40
50

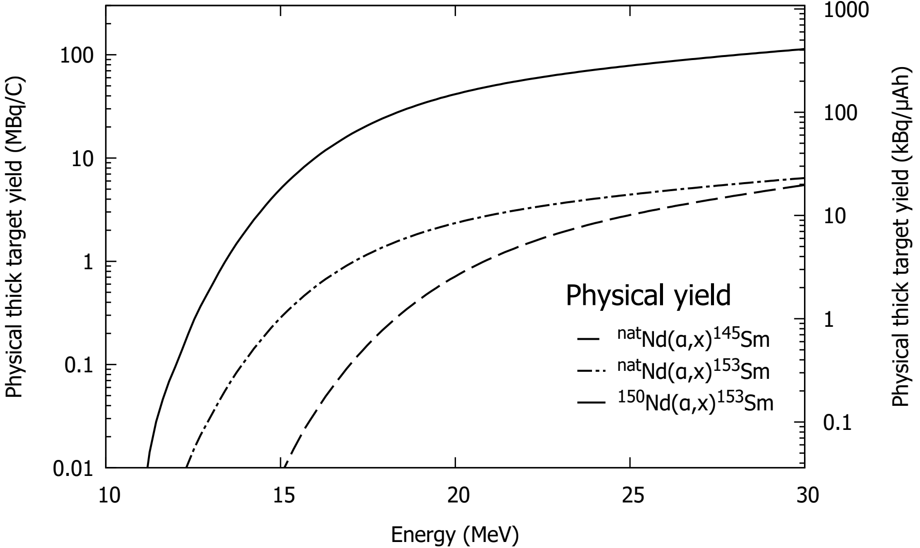

Physical thick target yield (MBq/C)
100
10
1
0.1
0.01
Physical thick target yield (kBq/μAh)
1000
100
10
1
0.1
10
15
20
25
30
Energy (MeV)
Physical yield
$^{nat}Nd(\alpha,x)^{145}Sm$
$^{nat}Nd(\alpha,x)^{153}Sm$
$^{150}Nd(\alpha,x)^{153}Sm$